PHYSICAL REVIEW B, VOLUME 65, 165329

Amorphization mechanism and defect structures in ion-beam-amorphized Si, Ge, and GaAs

J. Nord, K. Nordlund, and J. Keinonen
Accelerator Laboratory, P.O. Box 43, FIN-00014 University of Helsinki, Finland
(Received 31 May 2001; revised manuscript received 22 January 2002; published 10 April 2002)

We are studying ion-irradiation-induced amorphization in Si, Ge, and GaAs using molecular-dynamics simulations. Although high-energy recoils produce defects and amorphous pockets, we show that low-energy recoils (about 5–10 eV) can lead to a significant component of the athermal recrystallization of preexisting damage. For typical experimental irradiation conditions this recrystallization is, however, not sufficient to fully recrystallize larger amorphous pockets, which grow and induce full amorphization. We also examine the coordination and topological defect structures in Si, Ge, and GaAs observed in the simulations, and find that these structures can explain some experimentally observed features found in amorphous semiconductors. For irradiated amorphous GaAs, we suggest that long (about 2.8 Å) and weak Ga-Ga bonds, also present in pure Ga, are produced during irradiation.

DOI: 10.1103/PhysRevB.65.165329 PACS number(s): 64.70.Kb, 61.43.Dq, 61.72.Cc, 61.82.Fk

I. INTRODUCTION

Ion implantation of semiconductors at doses high enough to introduce significant amounts of electrically active dopants, normally first leads to amorphization of the implanted volume. Although the material is usually subsequently recrystallized by annealing, the mechanisms leading to amorphization may affect dopant clustering. The amorphization mechanisms have been intensively studied in the literature, see, e.g., Refs. 1–18. Still, the mechanisms leading to amorphization even in the most common semiconductor materials such as Si remain subject to debate. Early models attempted to describe amorphization by either pure defect accumulation (homogeneous) or direct impact (heterogeneous) models. Many recent models are a mixture of these two models, and take into account that some thermal recrystallization can occur during irradiation (see Ref. 15 and references therein).

It is also not clear whether the structure of the amorphous material produced by irradiation corresponds to that produced by other means, such as quenching. Some experiments indicate that at least the density of amorphous Si (a-Si) produced by ion beams is always the same or smaller than that of crystalline Si (c-Si) (Ref. 19), yet other experiments and computer simulations observe an a-Si phase denser than c-Si.[20,21] Custer *et al.* conclude this to indicate that the computer models describing Si by tetrahedrally coordinated atoms are erroneous.[19] This implies that the presence of overcoordinated and undercoordinated Si atoms in ion-beam-amorphized Si is responsible for the discrepancy.

Since it is probable that defects smaller than those visible in transmission electron microscopy experiments play a significant role in the amorphization process,[3] atom-level computer simulations can play a significant role in understanding the pathway to amorphization. Numerous computer-simulation studies have examined the amorphization and recrystallization mechanisms of Si from different viewpoints.[22,23,7–10,13,14,24,25] However, only a few of them have produced a-Si by multiple recoils in c-Si and studied the structure and density of a-Si. These studies have been limited to the use of only one interatomic potential[23] and in some cases the results have been partly dependent on simulation parameters with no experimental correspondence.[13,26]

In this paper we study the amorphization of Si, Ge, and GaAs by amorphizing the material with energetic self-recoils starting from pristine crystal. We use three different interatomic potentials for Si and two for Ge to confirm the reliability of the obtained results. In GaAs only one model capable of describing crystalline-to-amorphous phase transitions was available.

The paper is organized as follows. The simulation methods are explained in Sec. II. In Sec. III we first examine the effects of different recoil distributions (Sec. III A) and boundary conditions (Sec. III B) on the structure of the amorphous phase in Si. After that we examine amorphization (Sec. III C) and annealing in Si (Sec. III D). We then study those aspects of amorphization in Ge (Sec. III E) and GaAs (Sec. III F) that may differ from the behavior of Si. In the discussion (Sec. IV) we relate our results to analytical models and experiments.

II. METHOD

To study the properties of ion-beam-amorphized semiconductors we amorphized simulation cells by successive energetic recoils. Monoenergetic (100 eV or 1 keV) recoils as well as a continuous recoil energy distribution (from 3 or 15 to 2000 eV) were used. Periodic boundary conditions were used in three dimensions in all the simulations. The number of atoms was 22 000 for 1-keV recoils, 4000 and 8000 for 100-eV recoils, and 40 000 for the continuous recoil energy distribution.

In the *first phase* an energetic recoil was started at about the middle of the simulation cell, which was initially at 0 K temperature. The cell was cooled down towards 0 K at the borders using the Berendsen temperature control method.[27] Simulation times varying between 6000 and 10000 fs were used for the 1 keV energy to confirm that the final results do not depend on the simulation times used. The temperature after every recoil event was below 80 K. In the simulations with varying recoil energy the simulation times depended linearly on the recoil energy. A minimum simulation time of 500 fs was used. In this stage the size of the cell was not

 ©2002 The American Physical Society

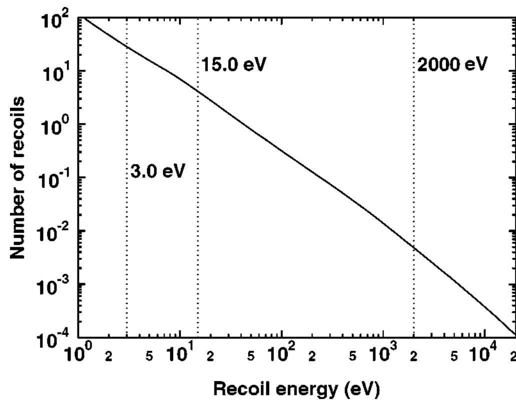

FIG. 1. The simulated recoil energy distribution of 500-keV Si bombardment of Si at 800–1200 Å depth. The dotted lines represent the selected cutoff values for amorphization simulations.

allowed to relax and a variable time step was used to speed up the simulations.

In the *second phase* the simulation cell was cooled to 0 K, and at the same time the pressure was relaxed with the Berendsen method[27] to 0 kbar in either all directions or in the z direction only (corresponding to experimental conditions where the irradiated area is bound from the sides). The relaxation times varied between 2000 and 3500 fs. In the continuous energy cases, the cell was relaxed after each 100 eV of accumulated deposited energy. After relaxation the atoms were displaced by a random distance in the x, y, and z directions, taking into account the periodic boundary conditions. This way all the positions were equal and we were able to generate a homogeneous distribution of the recoil energy in all parts of the cell.

The two-phase procedure was then iterated until full amorphization was achieved, i.e., when both the average potential energy and volume of the cell leveled out at some constant value. With this approach, the simulation results are not expected to depend on any parameters without some experimental correspondence. The simulation scheme is suitable to model ion irradiation for energies and ions where most of the recoils are well separated in space.

Monoenergetic 100 eV and 1 keV recoil energy distributions were used to study whether the structure or amorphization dose depends on the recoil energy. In order to obtain a continuous recoil energy distribution corresponding to typical experimental conditions, we selected recoils corresponding to an energy distribution produced by a 500-keV Si bombardment of Si, which is an implantation condition well known to amorphize Si.[28] Only recoils produced in the depth region of 800–1200 Å were included. The recoil energy distribution was obtained with the MDRANGE method.[29,30] The distribution is illustrated in Fig. 1.

Because very low-energy recoils ($E\sim1$ eV) are dominant, recoils with energies higher than 3 and 15 eV were considered. We denote this minimum recoil energy by $E_{\mathrm{rec,min}}$. The latter value was chosen because it is approximately the threshold displacement energy in Si.[31,32] Recoils with energies below this do not affect the damage structure in initially perfect crystal regions. After the observation that recoils at energies close to the threshold energy can cause some dynamic recrystallization of the material (see below), we also used $E_{\mathrm{rec,min}}=3$ eV in some simulations. This value was chosen because it is lower than the strength of two bonds in Si, so recoils below this value should not cause any significant structural change even in a-Si. In simulations with $E_{\mathrm{rec,min}}=3$ eV the cell amorphized somewhat slower, but the final a-Si structure was practically identical with the simulations with $E_{\mathrm{rec,min}}=15$ eV. Since the *computing* time needed to achieve full amorphization was very much longer for 3 eV minimum energy (because of the large number of low-energy recoils), $E_{\mathrm{rec,min}}=15$ eV was used in most simulations.

Recoils at energies higher than 2 keV were not used. This allowed us to limit the size of the simulation cells and speed up the calculations. We justify this approximation by noting that recoils above ~2 keV break down into subcascades,[33,34] so no new types of damage states are produced by higher-energy recoils.

The primary damage state produced in individual cascades has been extensively studied in the literature.[7,14,23,31–37] The simulations by Caturla *et al.* have shown that the damage states produced in Si by ion irradiation are strongly dependent on the mass of the ion.[7] For light ions, such as B, about 20–30 % of the defects are isolated. The heavier ions produce more concentrated damage, but even for As the fraction of isolated defects is higher than 5%. This shows that there is some homogeneous amorphization during ion irradiation. The damage produced in germanium is much more localized than in silicon.[34] Less than 2% of the defects produced by 10-keV recoils are isolated, and over 95% lie in clusters larger than six atoms. Therefore germanium has a stronger tendency towards direct impact amorphization. Like silicon, many isolated defects are also produced in GaAs by self-recoils.[37] Over 10% of the defects are isolated in the recoil energy range 400 eV–10 keV, and about 60% of the damage is in clusters larger than six atoms. A combination of heterogenous and homogenous amorphization mechanisms would, therefore, be favored at low temperatures in the initial stages of the process in GaAs.

The angular distribution was simulated for both 100-eV and 1-keV recoils, and the amorphizations were studied both by using a simulated angular distribution and random directions of recoils.

Several amorphization runs were repeated to be sure that the conclusions were not affected by statistical fluctuations. Amorphous material was also generated by melting and quenching. First the material was kept at a temperature much higher than its melting point (3000–5000 K) for 50–100 ps. The cell was then cooled down to 0 K not faster than 0.01 K/fs. The melting and quenching was then repeated using a starting temperature lower by about a factor of 2. This procedure was repeated until the starting temperature was lower than 400 K. The quenching ratio is still high compared to experimental conditions, so the effect of the simulation time was estimated by running a quenching simulation for longer than 3 ns for comparison purposes. The differences between quenched and irradiated materials remained qualitatively the same. To acquire sufficient statistics, 8000 atoms were used in the quenching simulations.

The forces between atoms were described by semiempirical many-body potentials. The Stillinger-Weber (SW) potential,[38] Tersoff III (T-III) potential,[39] and environment-dependent interatomic potential[40–42] (EDIP) were used for Si, the SW (Refs. 38 and 43) and Tersoff[44] (T) potentials for Ge, and a potential by Albe *et al.*[45] (ANNK) for GaAs.

Since, contrary to the Si and Ge potentials, the properties of the GaAs potential are not widely known, we comment here on some of the features relevant to this study. Additional details can be found in Ref. 45.

The GaAs potential has been fitted to several GaAs, As, and Ga phases. Even the complex Ga ground-state structure is reproduced. The potential describes many common defects reasonably and phase transitions were considered during the development process.

The compound nature of GaAs makes the generating of amorphous GaAs by melting more difficult than that of Si or Ge. In liquid GaAs, the As and Ga components segregate partially, and As bubbles are formed in the liquid. Even with simulation times up to 10 ns we were not able to generate homogeneous amorphous GaAs. Therefore we only compared the irradiated amorphous GaAs to its annealed version.

The structure of amorphous materials was characterized by the distribution of bond lengths, potential energies of atoms, and angles between bonds. Coordination defects or atoms with a high potential energy were considered to be defects in the amorphous state. The amorphization dose for different cases could easily be obtained, as well as the density of the amorphous material.

III. RESULTS

A. Effect of recoil impact vector

The possible effects of the recoil angle and energy distributions on the structure of the amorphous material were tested with the T-III potential for Si. The effects of the recoil velocity vector direction were studied for 100-eV and 1-keV recoils with two different angular distributions. One distribution used the same probability for all directions, while the other one used the angular distribution obtained in MDRANGE simulations. No difference was observed between materials produced by angle-dependent and random direction recoils. The energy doses needed for full amorphization were the same, as well as the dependencies between the volume and dose, and potential energy and dose.

The volume change was found to depend strongly on the energy of the recoil atoms (see Figs. 2 and 3 and Table I). For monoenergetic 100-eV recoils the volume change was bigger than for 1-keV recoils. The observation that there are more high-energy defects per deposited energy for the 100-eV recoils is not surprising. This is explained by the fact that the local, in-cascade heating produced by cascades can recombine defects.[9] Since the 1-keV recoils deposit more kinetic energy, the heating and possibilities for defect recombination are larger in this case. This effect is analogous to cascades in metals, where it is well known that with increasing cascade energy an increasingly large fraction of defects will recombine.[46] In semiconductors the effect is less pronounced because of the nature of the chemical bonding.[9,34]

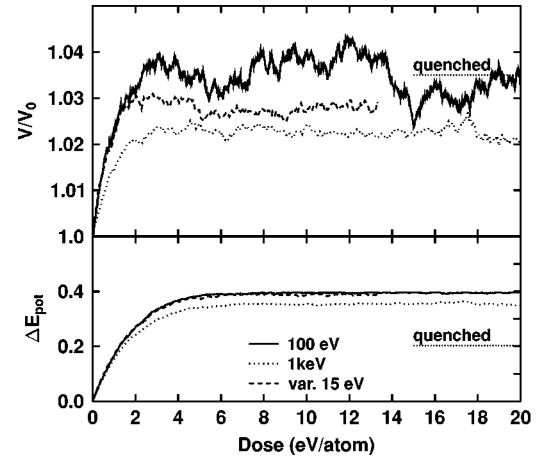

FIG. 2. Development of volume and potential energy compared to the perfect Si crystal in 100-eV and 1-keV monoenergetic irradiations, and a variable energy irradiation with 15 eV minimum recoil energy shown as a function of irradiation dose. Values for quenched amorphous material are included for comparison purposes. The EDIP potential model was used.

A continuous recoil energy distribution was also used in simulations with EDIP and T-III. With $E_{\mathrm{rec,min}}=15$ eV, the potential-energy development is very similar to the 100-eV case. For T-III this is also true for the development of the volume, whereas for EDIP the volume with the continuous distribution saturates to a lower value. Two different minimum recoil energies $E_{\mathrm{rec,min}}$, 3 and 15 eV, were used for variable recoil energy simulations for the T-III potential model. The final volume and average potential energy of the amorphized materials were the same for both values of $E_{\mathrm{rec,min}}$, but the 3-eV case amorphized slower. The potential-energy saturation dose was the same for the variable energy scheme with $E_{\mathrm{rec,min}}=15$ eV as for all the tested monoenergetic cases. For $E_{\mathrm{rec,min}}=3$ eV the dose was somewhat

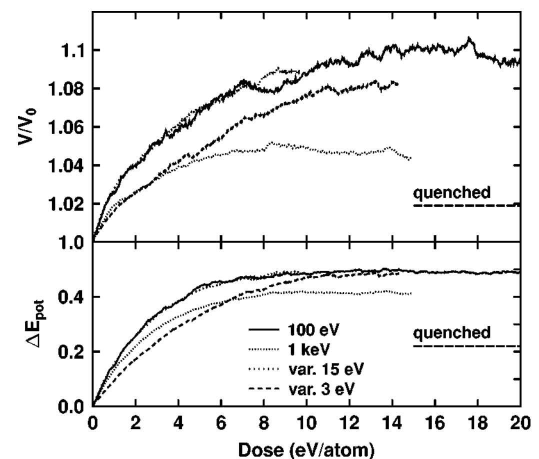

FIG. 3. Development of volume and potential energy compared to the perfect Si crystal in 100-eV and 1-keV monoenergetic irradiations, and variable energy irradiation with 3 and 15 eV minimum recoil energies as a function of irradiation dose. Values for quenched amorphous material are included for comparison purposes. The T-III potential model was used.

TABLE I. Amorphization doses for different cases for Si potentials. E_{dose} is the dose needed to reach a saturation potential-energy level and V_{dose} is the dose per atom needed for the final volume. The column "relaxation" denotes pressure relaxation in all directions (3D), one direction (z), or to an annealing temperature. V/V_0 is the volume of the amorphized material compared to a perfect crystal and $E_{potential}$ is the average potential energy for an amorphous structure.

Method	Relaxation	E_{dose} (eV)	V_{dose} (eV)	V/V_0	$E_{potential}$ (eV)
		EDIP			
100-eV irr.	z	6.5	10	1.036	-4.26
100-eV irr.	3D	6.5	2	1.035	-4.25
1-keV irr.	3D	6.5	3	1.022	-4.29
Variable E irr.[a]	3D	6.5	2	1.029	-4.26
Quench				1.035	-4.40
Variable E irr.[a]	900 K			1.036	-4.46
		T-III			
100-eV irr.	3D	8	12	1.095	-4.13
100-eV irr.	z	8	13	1.093	-4.13
1-keV irr.	3D	8	7	1.047	-4.20
1-keV irr.	z	8	13	1.045	-4.20
Variable E irr.[a]	3D	8	8	1.089	-4.13
Variable E irr.[b]	3D	11	11	1.08	-4.14
Quench				1.019	-4.40
		SW			
1-keV irr.	3D	17	17	0.947	-4.09
Quench				0.944	-4.11
Expt.		12 [c]		1.018 [d]	

[a] $E_{rec,min} = 15$ eV.
[b] $E_{rec,min} = 3$ eV.
[c] Reference 1.
[d] Reference 19.

higher. The reason behind this is that low-energy recoils with $\sim 5-10$ eV energy recrystallize the material (see Sec. IV).

B. Effect of pressure boundary conditions

Another condition that might generate direction dependency in the structure is the pressure relaxation. In the second phase, the relaxation phase of the amorphization simulations, the pressure was allowed to relax to zero in all directions separately, or in the z direction only. While the development of the average potential energy along with the amorphization dose was unaffected by the relaxation condition, the volume change in the latter case was slower. When the pressure was relaxed only in one direction, more irradiation was needed for the pressure to relax in the x and y directions. For most cases the volume and average potential energy did not saturate at the same dose. Therefore, the volume is not a good measure for the amorphization of the material. The final potential energy and volume were the same in both relaxation schemes.

C. Amorphization in Si

Semiempirical interatomic potentials have different functional forms and are fit to different sets of properties. It is not clear which, if any, of the potentials is suitable for simulating a certain phenomenon that is not a part of the original fitting database. The problem is especially important in simulations of disordered phases, since functional forms are often built on the basis of favoring some bond angle in a well-defined and ordered crystal lattice. Therefore, we repeated the amorphization simulations with the three potentials T-III,[39] EDIP,[42] and SW (Ref. 38) for Si. The reliability of the results for the potentials was estimated by comparing experimental values for an amorphization dose and density with the simulated ones.

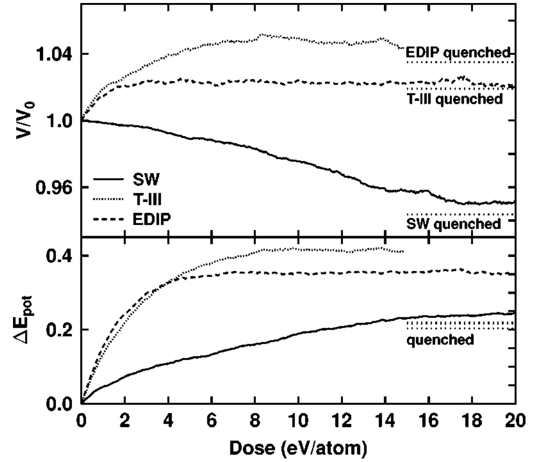

FIG. 4. Development of volume and potential energy compared to the perfect Si crystal during ion irradiation for different Si potential models as a function of irradiation dose. 1-keV monoenergetic recoils were used.

Large potential dependent differences were found in the density of a-Si. The EDIP and T-III potential models were able to reproduce the positive volume change observed in the experiments,[19] whereas for SW the amorphous material was denser than c-Si. The volume-dose dependency for different potentials for 1-keV monoenergetic recoils is shown in Fig. 4.

The distribution of the potential energies of the atoms is illustrated in Fig. 5. The difference between the amorphization methods (quenching from a melt vs irradiation) was largest for EDIP and smallest for SW. For all three potential models the average potential energy was higher for the irradiated case than for the quenched one. This shows that defects of the amorphous structure are present in the irradiated cells.

Because the quenching method may be sensitive to the quenching ratio and simulation time, the procedure was repeated for different time scales. Longer simulation times only increased the difference between the structures of molten and irradiated materials, confirming that the difference exists regardless of the quenching time. The longest quenching simulation time was about 3 ns.

For all the tested Si potentials and irradiation conditions the average coordination was bigger and average bond length longer in irradiated than in quenched cases, as shown in Table II and Fig. 6. The average bond lengths for different irradiation conditions were about 2.47 Å for EDIP and about 2.43 Å for T-III and SW. Over 90 % of the atoms in the

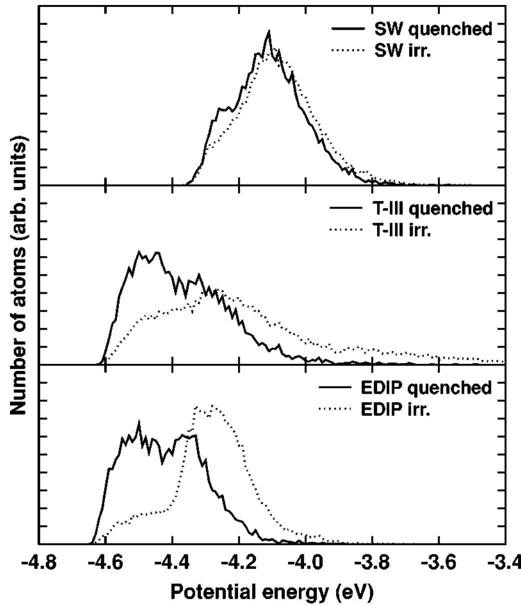

FIG. 5. Potential-energy distribution for different Si potential models. The dotted line represents the distribution for amorphized material produced by 1-keV monoenergetic recoils, and the solid line represents the distribution for quenched amorphous material.

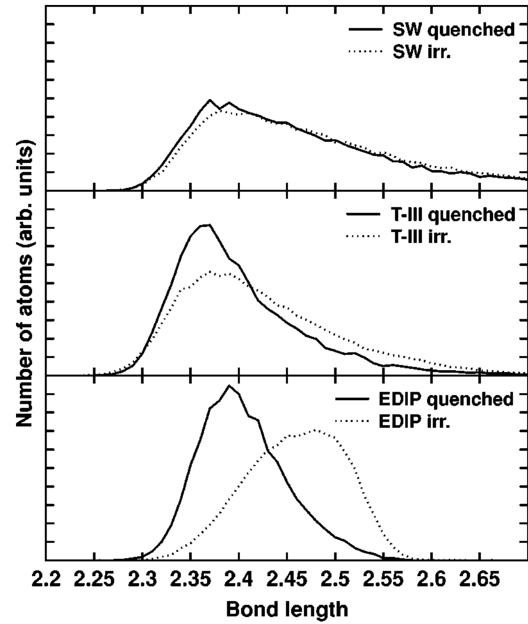

FIG. 6. Bond-length distributions of amorphous materials for the different Si potential models. The dotted line represents the distribution for amorphized material produced by 1-keV monoenergetic recoils and the solid line represents the distribution for quenched amorphous material.

quenched amorphous structures described by the EDIP and T-III potential models had a coordination of 4, and the average coordination number was a little higher than 4. For irradiated structures described by EDIP the most common coordination was 5 and by T-III, 4. SW produced a very similar structure for both irradiated and quenched cells. The pair-correlation functions in Fig. 7 show increased ordering in the molten structure at a second peak near 4 Å for the T-III and EDIP potential models. The SW model has an additional peak just above 3 Å, which is not observed in the experimental function, for both molten and irradiated structures. The pair-correlation functions of the EDIP and T-III models, which do not have a strong peak at 3 Å, are in good agreement with the experimental curve.

The bond-angle distributions of irradiated and molten structures are illustrated in Fig. 8. Once again the SW model has about the same distributions for both production methods. However, the EDIP model shows sharp peaks near 60° and 75°. The T-III model also shows a small increase near these values. The 60° peak is associated with a Si-Si-Si triangle with angles near 60°. There are many more three-rings

TABLE II. Number of three-membered rings, coordination distribution (Z values), average bond length $\langle R_{bond}\rangle$, and coordination $\langle Z\rangle$ for different Si potential models and amorphization methods.

Method	Three rings/atom	$Z=3$	$Z=4$	$Z=5$	$\langle Z\rangle$	$\langle R_{bond}\rangle$
	EDIP					
Irr. 100 eV	0.137	0.5	34.0	65.3	4.67	2.47
Irr. 1 keV	0.108	0.2	44.8	54.8	4.55	2.46
Irr. variable energy	0.137	0.5	39.1	60.0	4.60	2.47
Quenched	0.005	0.1	93.9	6.0	4.06	2.40
	T-III					
Irr. 100 eV	0.013	10.9	64.3	22.8	4.15	2.43
Irr. 1 keV	0.010	7.6	65.5	24.8	4.21	2.43
Irr. variable	0.014	10.2	64.9	22.9	4.16	2.43
Quenched	0.001	0.5	91.4	8.1	4.08	2.39
	SW					
Irr. 1 keV	0.0003	0.9	53.8	43.1	4.46	2.48
Quenched	0.0003	0.7	56.5	41.1	4.43	2.47

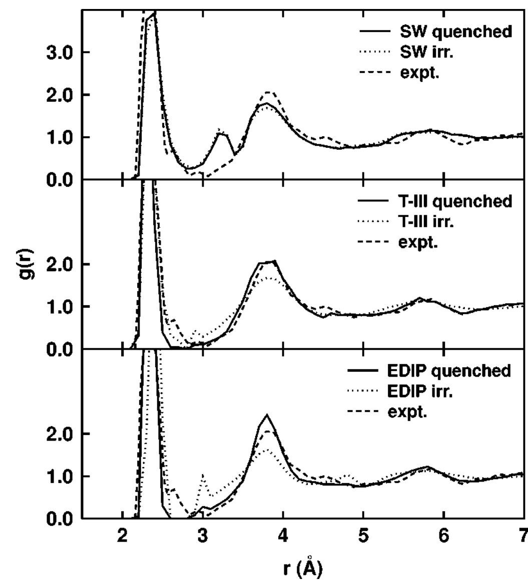

FIG. 7. Simulated and experimental[20] pair distribution functions for amorphous silicon. 1-keV monoenergetic recoils and SW, T-III, and EDIP potential models were used.

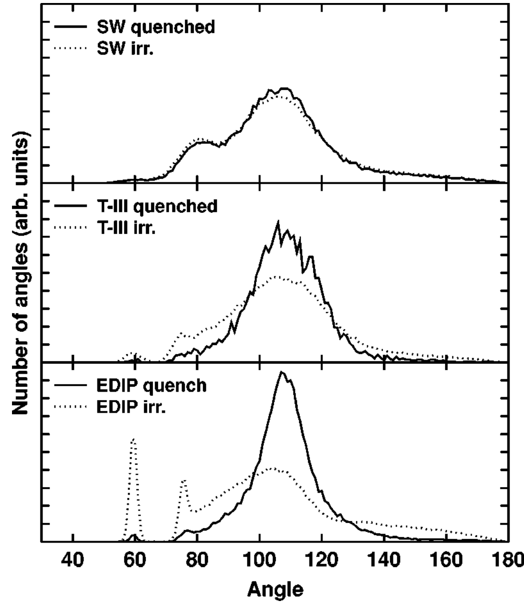

FIG. 8. Distribution of angles between bonds for different Si potential models. The dotted line represents the distribution for amorphized material produced by 1-keV monoenergetic recoils and the solid line represents the distribution for quenched amorphous material.

in irradiated structures, as shown in Table II. The peak near 75° is associated with four-membered rings, which often have two 75° angles.

The amorphization energy doses needed to saturate both the volume and potential energy vary between 6 and 17 eV/atom for different Si potential models and amorphization methods. These values are in a reasonable agreement with the experimental value of about 12 eV/atom (Ref. 1) determined at low temperatures where defect migration is not important.

D. Stability of *a*-Si

The stability of the structure of *a*-Si produced by irradiation was tested by heating amorphous cells up to 300, 600, 900, and 1200 K. The cells were held at each temperature for about 4 ns and then quickly cooled down to 0 K. The initial cell for annealing simulations was amorphized by variable energy recoils with $E_{\mathrm{rec,min}} = 15$ eV. We focused on the *T*-III and EDIP potentials, as the SW potential predicted a density of the amorphous material in clear contradiction to the experiments.

After annealings at 600 and 900 K the structure of the cell modeled by EDIP was very close to the quenched amorphous structure, as shown in Table III. The average coordination numbers, potential energies, and volumes are almost the same for annealed and quenched materials. The numbers of three- and four-membered rings are also at the same level and qualitative differences are not present in the bond-angle distributions. At 1200 K the fraction of fivefold coordinated atoms suddenly increases to about 26%. This is probably because 1200 K is above the glass temperature of EDIP for Si, which we determined to be <1200 K (Ref. 47).

TABLE III. Percentage of most common coordinations (Z values), and average bond length $\langle R_{bond} \rangle$ and coordination $\langle Z \rangle$ of irradiated *a*-Si modeled by EDIP or *T*-III for variable energy recoils with 15 eV minimum recoil energy before and after annealing. Values for quenched *a*-Si are included for comparison purposes.

Anneal	$Z=3$	$Z=4$	$Z=5$	$\langle Z \rangle$	$\langle R_{bond} \rangle$	E_{pot}	V/V_0
				EDIP			
Before	0.45	39.1	60.0	4.60	2.47	-4.26	1.028
300 K	0.06	66.9	33.0	4.32	2.43	-4.36	1.009
600 K	0.08	91.0	9.0	4.09	2.40	-4.42	1.032
900 K	0.06	96.1	3.8	4.04	2.39	-4.45	1.037
1200 K	0.21	73.5	26.2	4.26	2.43	-4.36	1.012
Quench	0.05	93.9	6.0	4.06	2.40	-4.44	1.035
				T-III			
Before	10.2	64.9	22.9	4.16	2.43	-4.14	1.089
300 K	6.32	71.5	20.9	4.17	2.42	-4.21	1.066
600 K	2.38	79.4	17.6	4.16	2.41	-4.30	1.030
900 K	1.06	86.4	12.4	4.12	2.40	-4.36	1.025
1200 K	0.81	91.3	7.8	4.07	2.39	-4.39	1.035
Quench	0.5	91.4	8.1	4.08	2.39	-4.40	1.019

The number of coordination defects in annealed cells modeled by the *T*-III potential decreases during annealing. The coordination number distribution after the 1200-K annealing of the irradiated cell is similar to that in the quenched cell. The bond-angle and potential-energy distributions are also similar. However, the amorphous structure produced by quenching is about 1.6% denser than the annealed cell, and has 2.4% less four-membered rings.

E. Amorphization in Ge

The SW (Refs. 38 and 43) and *T* (Ref. 44) potential models were used for Ge. The irradiated amorphous Ge (*a*-Ge) described by the SW potential was less dense than molten *a*-Ge, and crystalline Ge (*c*-Ge) was denser than both of them. The decrease in the density is explained by longer bonds, which were about 3% longer in irradiated material than in *c*-Ge, as can be seen in Table IV. The average coordination number was very close to that of *c*-Ge, 4.04 for the irradiated and 4.02 for the molten cell (Table IV). The development of volume during irradiation is shown in Fig. 9 for both potential models.

TABLE IV. Percentage of most common coordination numbers (Z values), and average bond lengths $\langle R_{bond} \rangle$ and coordination $\langle Z \rangle$ in *a*-Ge cells modeled by the SW and *T* potentials.

Material	$Z=3$	$Z=4$	$Z=5$	$Z=6$	$\langle Z \rangle$	$\langle R_{bond} \rangle$
c-Ge	0.0	100.0	0.0	0.0	4.00	2.45
Irr. SW Ge	2.4	91.5	6.07	0.0	4.04	2.52
Melt SW Ge	1.1	96.2	2.8	0.0	4.02	2.50
Irr. *T* Ge	1.7	33.8	40.3	18.4	4.93	2.56
Melt *T* Ge	0.3	80.0	17.4	2.1	4.21	2.50

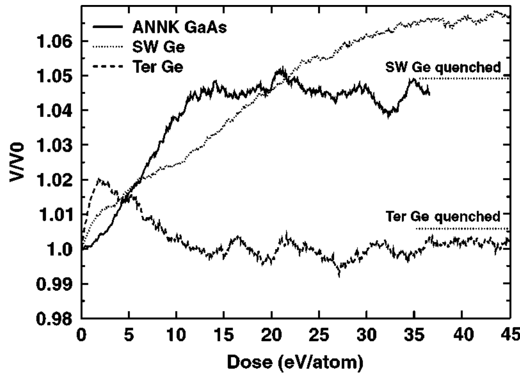

FIG. 9. Development of volume in different Ge and GaAs potential models as a function of the irradiation dose. Monoenergetic 1-keV recoils were used to produce irradiated amorphous material. Values for quenched material are included for the Ge models.

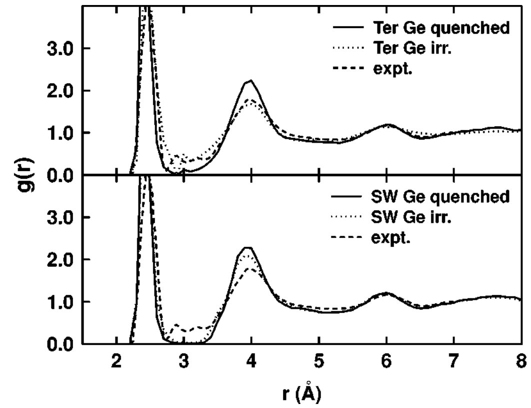

FIG. 10. Simulated and experimental pair distribution functions for amorphous germanium. 1-keV monoenergetic recoils and T or SW potential models were used in the simulations.

The behavior of Ge during ion irradiation described by the T potential is more complicated. First the volume increases, and then decreases almost back to the level of c-Ge. The bonds are about 4% longer than in c-Ge, but highly coordinated atoms compensate for the change in volume. After the material was fully amorphized by irradiation, the average coordination was 4.93 (Table IV). Molten a-Ge has a lower coordination of 4.21 and is slightly less dense than c-Ge.

Experimentally the coordination number of irradiated a-Ge was found to be close to 4.[48] The *ab initio* calculations predict that the coordination number of molten a-Ge is 4.05.[49] These are in a good agreement with our amorphization simulations carried out with the SW potential, which predict a small increase in coordination number. The simulations with the T potential show more increase in the coordination number for both the molten and irradiated amorphous materials. The bonds are found to be longer in irradiated cells than in quenched ones. This is in agreement with the experiments, where the bond length is found to decrease during annealing.[50] Our simulations predict longer bonds than those found experimentally. However, the experimental bond length increased with ion dose.[48] The simulated pair-correlation functions, especially that of irradiated Tersoff a-Ge, are in a good agreement with the experimental ones (see Fig. 10).

For molten a-Ge described by the SW potential, the angles between the bonds are distributed near 108.6°, with a standard deviation of 10.8°. The average angle for irradiated material is 108.3° with a standard deviation of 13.1°.

The amorphization dose for the T Ge potential model is 9.1 eV/atom (Table V), which is in a good agreement with the experimental value of about 13 eV/atom [calculated from irradiation parameters in Ref. 48 using SRIM (Ref. 51) to obtain the deposited energy]. The SW Ge overestimates the amorphization dose probably because it has a melting point that is too high.[34]

F. Amorphization in GaAs

Amorphization in GaAs was modeled by a potential by Albe *et al.*[45] For this potential we could not obtain molten amorphous GaAs, as explained in Sec. II. Therefore, we compare the irradiated a-GaAs with a structure obtained by annealing the irradiated a-GaAs at a temperature much lower than the melting point.

We simulated ion-beam-induced amorphization in GaAs by successive 1-keV recoils (randomly chosen as Ga or As). The amorphization dose was about 13 eV/atom (Table V), which is in a reasonable agreement with the experimental value of about 10 eV/atom (obtained from the low-temperature values in Fig. 5 of Ref. 52). Crystalline GaAs (c-GaAs) was about 4.5% denser than irradiated a-GaAs.

The distribution of Ga-Ga, As-As, and Ga-As bonds before and after annealing are shown in Fig. 11. Most of the bonds are between Ga and As atoms. The fraction of wrong bonds before annealing was 37%. About 73% of the wrong bonds were Ga-Ga bonds with an average length of 2.81 Å. These bonds are longer versions of the metallic bonds present in pure Ga.[53] The number of covalent wrong bonds was about 14%. If the cutoff value for the coordination number calculation is selected as 2.7 Å (cf. Sec. IV C), the average coordination is 3.45. If also longer Ga-Ga bonds are counted, the coordination number is 4.64.

The amorphized cell was annealed at 900 K for 400 ps and then cooled to 0 K. During the annealing, the number of Ga-As bonds increased by about 2.5%. The number of Ga-Ga bonds near 2.8 Å decreased by about 13% to 24%, indicating that these bonds are not stable at high tempera-

TABLE V. Amorphization dose for saturation volume (V_{dose}), potential energy (E_{dose}), volume (V/V_0), and potential energy (E_{pot}) of amorphous material compared to a perfect crystal for the Ge and GaAs potential models.

Material	E_{dose} (eV)	V_{dose} (eV)	V/V_0	E_{pot}
Irr. T Ge	9.1	9.1	1.000	-3.42
Melt T Ge			1.006	-3.58
Irr. SW Ge	36	36	1.067	-3.48
Melt SW Ge			1.049	-3.54
Irr. GaAs	13	12	1.045	-2.89
Annealed GaAs			1.029	-2.98

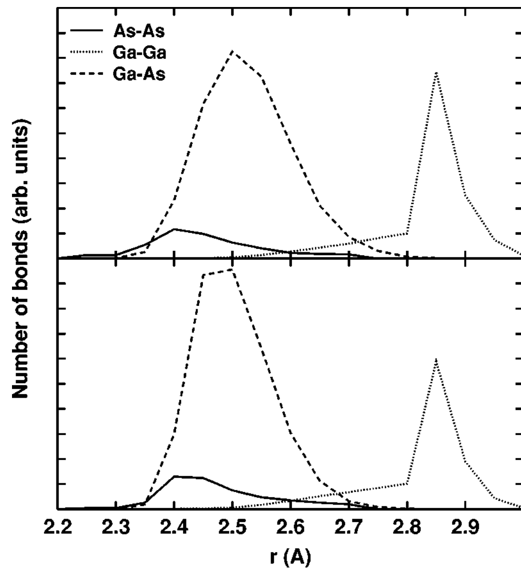

FIG. 11. Simulated bond-length distributions of As-As, Ga-Ga, and Ga-As in ion-irradiated amorphous GaAs. Monoenergetic 1-keV recoils were used and the interactions were modeled by the ANNK potential. The upper figure depicts the case before annealing and the lower after annealing.

tures. There were some more As-As bonds after annealing, and As segregation was observed. However, simulations at temperatures of 1300 and 1500 K (still below the melting point of about 1900 K for the potential model) showed that the As regions are not stable and can be annealed at longer time scales. Because the As regions can be annealed, it is also possible that all Ga defects with bond lengths 2.8 Å are converted to Ga-As bonds during long enough high-temperature annealing.

During annealing the average Ga-As bond length was shortened from 2.51 to 2.48 Å. At the same time the length of As-As bonds increased from 2.44 to 2.46 Å. The number of covalent bonds shorter than 2.7 Å increased during annealing.

IV. DISCUSSION

We first emphasize that the results for the amorphization mechanisms during ion irradiation presented here are directly relevant only to low-temperature experiments [lower than 150 K for Si (Refs. 54–56) and Ge (Ref. 57), and 200 K for GaAs (Refs. 58 and 59)], because at higher temperatures, defects in highly irradiated materials are mobile.

A. Amorphization mechanism

We first compare our results on amorphization in Si to those of some previous studies. Caturla *et al.*[22] have shown that 15-eV recoils can recrystallize a-Si when launched at the crystalline side of an amorphous/crystalline interface. Stock *et al.*[23] have reported that very low energy recoils (50 eV) do not amorphize Si modeled by Stillinger-Weber potential completely, and can in some cases cause partial recrystallization of the damage. Both observations are in good qualitative agreement with our observations that low-energy recoils can induce recrystallization during ion irradiation. However, for the reasons noted in Sec. III D (see also Ref. 60, where negative pressure had to be applied while producing a-Si by a melting-quenching method) the Si SW model does not give a very good description of amorphization, so a quantitative comparison with these previous results is not useful.

The discussion in the remainder of this section is based on the continuous 500-keV Si recoil spectrum, since this corresponds to experimental conditions. Because the recoil spectra of ions with similar masses do not differ greatly, the qualitative conclusions obtained here can be expected to also hold for other keV irradiating ions in the same mass range as Si.

The amorphization process is illustrated in Fig. 12. In this simulation the minimum recoil energy $E_{\mathrm{rec,min}}$ was set at 3 eV, and most recoil atoms have lower energies than 10 eV. These low-energy recoils can recombine defects by knocking interstitials into vacancies or intermediate states, which then spontaneously recombine.[61] An example of defects that are removed is circled in parts (a) and (b) of Fig. 12. If the defect concentration in some region is high enough, an amorphous region is formed. The region then starts to grow, because low-energy recoils cannot crystallize material inside amorphous pockets. One such region can be seen in the middle left side of the pictures in Fig. 12. On some occasions we observed partial recrystallization at the amorphous-crystalline interface, as predicted by previous studies.[22,24,25] But for this kind of recoil spectrum the effect is not strong enough to recrystallize the pockets completely. In the intermediate stages between crystalline and fully amorphized states, the material is observed to contain amorphous regions with some isolated defects between them. This is consistent with experiments in which amorphous zones are found to grow preferentially at the crystalline-amorphous interface[62] or at preexisting defects.[63]

Primary damage state simulations have shown (cf. Sec. II) that the damage produced by a single ion is both in the form of amorphous clusters and isolated point defects. Hence these cannot conclusively determine which mechanism dominates during prolonged irradiation. The simulations on prolonged irradiation described in this work show that the observed amorphization mechanism is not homogeneous (i.e., due to defect accumulation everywhere), because clear amorphization centers exist. On the other hand, the mechanism requires multiple ion passes in a spatial region before full amorphization, so the direct impact (heterogeneous) amorphization model does not directly apply either. We thus interpret the mechanism to be a combination of the heterogeneous and homogeneous mechanisms.

In the simulations with continuous recoil energy distribution and $E_{\mathrm{rec,min}} = 15$ eV, the damage is not recombined as much, and the amorphization proceeds via frozen-in damage accumulation. This was also true for all monoenergetic simulations. These observations prove that the recombination observed is predominantly due to the low-energy ($E < 15$ eV) recoils. For heavier ions or target materials this mechanism may be favored, since the damage is more concentrated.

We use three different analytical models predicting the development of the amorphous fraction as a function of the

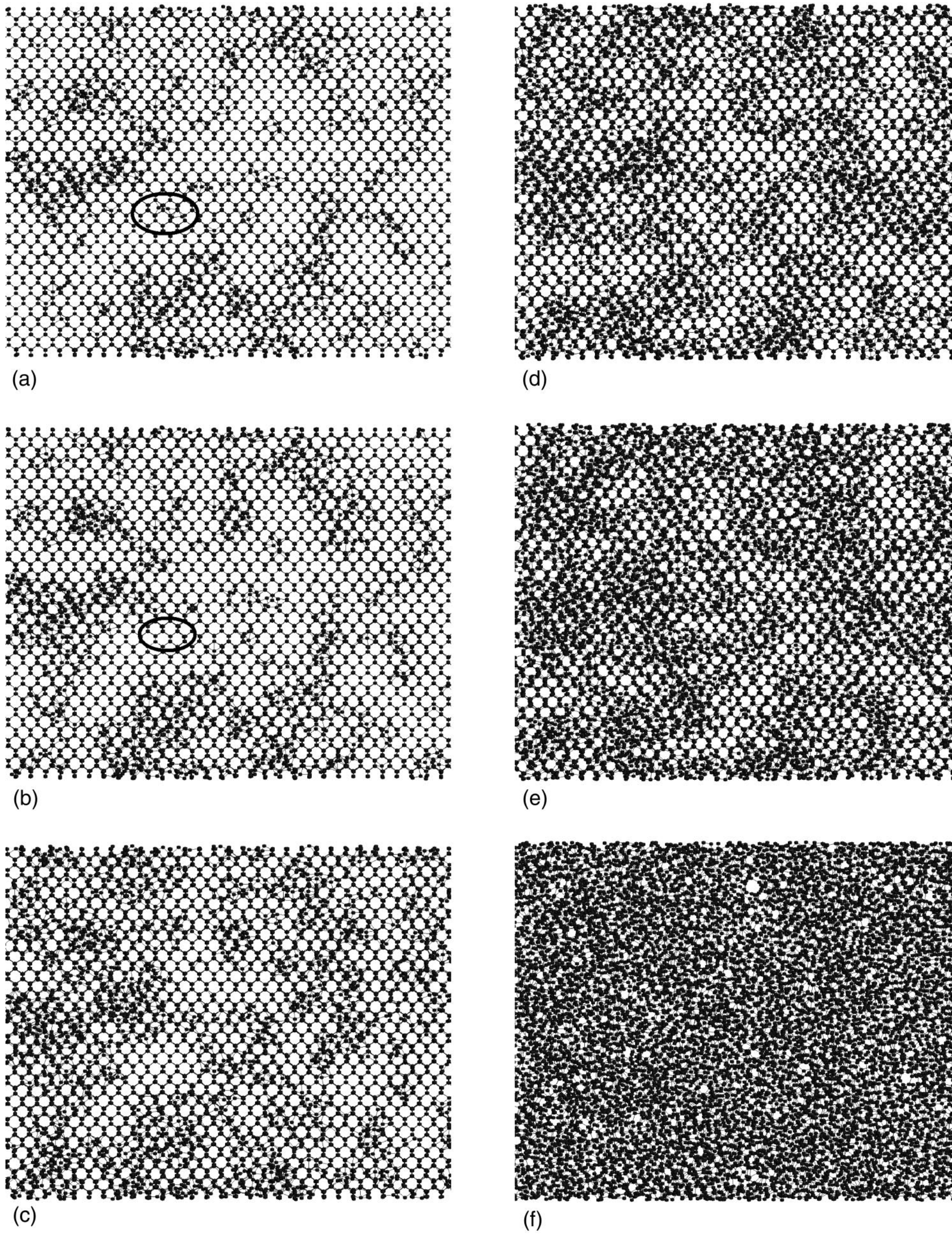

FIG. 12. A four-unit-cell-thick cross section of the simulation cell in a (110) plane during ion irradiation of Si. The doses are (a) 1.1 eV/atom, (b) 1.5 eV/atom, (c) 2.8 eV/atom, (d) 4.2 eV/atom, (e) 5.6 eV/atom, and (f) 14 eV/atom. An example of defect recombination is circled in (a) and (b). The T-III potential model and simulated recoil energy distribution with 3 eV minimum recoil energy were used.

dose to help interpret the amorphization mechanism. The amorphous fraction was defined as follows. The structure factor P_{st} (Ref. 9) is calculated for each atom i,

$$P_{st}=\frac{1}{p_u(i)}\left(\sum_j\left[\theta_i(j)-\theta_i^p(j)\right]^2\right)^{1/2}, \tag{1}$$

$$p_u(i)=\left(\sum_j\left[\theta_i^u(j)-\theta_i^p(j)\right]^2\right)^{1/2}, \tag{2}$$

where $\theta_i(j)$ are the angles formed between the atom i and its neighbors. $\theta_i^p(j)$ is the distribution of angles in a perfect lattice and $\theta_i^u(j)=j\pi/4(4-1)/2$ is the uniform angular distribution. Before performing the sum over angles, the $\theta_i(j)$ lists are sorted by magnitude. All atoms for which P_{st} is larger than 0.125 are considered "defect" atoms. If a "defect" atom has at least three defect neighbors, it is defined as amorphous. The amorphous fraction is the normalized amount of amorphous atoms.

The Gibbons direct impact model describes amorphization by direct impacts. The amorphous fraction f_a is[15]

$$f_a=1-\exp(-\sigma_a D), \tag{3}$$

where σ_a is the amorphization cross section and D is the amorphization dose. The model poorly describes the simulated development of an amorphous fraction, as seen in Fig. 13.

The recrystallization efficiency can be estimated by the amorphization process theory of Wang *et al.*[18] The theory assumes that the amorphization proceeds by direct impacts, but takes simultaneous crystallization into account. In the

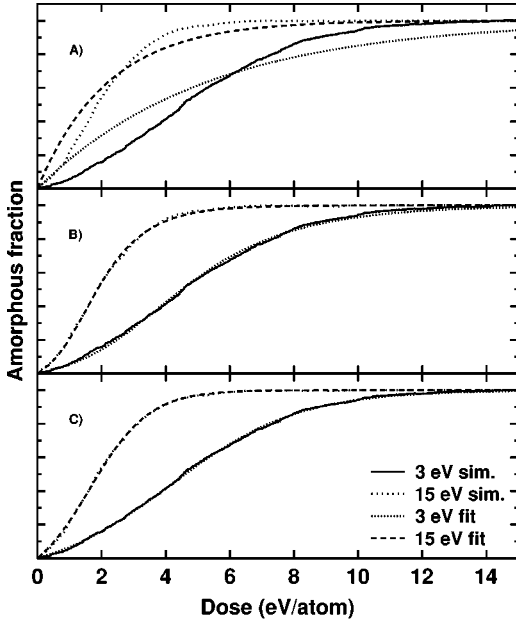

FIG. 13. Simulated amorphous fraction during ion irradiation of silicon and fits to (a) direct impact, (b) direct impact with crystallization, and (c) direct impact/defect stimulated models. The Tersoff-III potential model and recoil energy distributions consisting of 3 eV–2 keV or 15 eV–2 keV recoils were used.

Wang model the amorphous fraction f_a can be expressed as a function of a normalized ion dose D_n and crystallization efficiency A,

$$f_a = 1 - \frac{1}{\sqrt{A + (1-A)\exp[2(1-A)D_n]}}. \quad (4)$$

We fitted the parameters A and $k = D_n/D$, where D is the irradiation dose in energy/atom, for both $E_{\mathrm{rec,min}} = 3$ and 15 eV to see how the crystallization parameter is affected by low-energy recoils. We obtained a recrystallization parameter A of 0.9002 ± 0.0002 for the 3-eV case and 0.8667 ± 0.0008 for the 15-eV case. This indicated that there is more recrystallization with the lower-energy recoils included. The k parameter was (3.822 ± 0.009)/eV for 3 eV and (6.326 ± 0.049)/eV for 15 eV minimum recoil energy. Plots of the fits and original values are shown in Fig. 13. The model describes the development of the amorphous fraction much better than the Gibbons direct impact model.

The Hecking model[4] (used recently by Gao, Weber, and Devanathan[17] in simulations of SiC) describes amorphization by simultaneous direct impact and defect stimulated (growth of amorphous regions) methods. The analytical expression is[15]

$$f_a = 1 - \frac{\sigma_a + \sigma_s}{\sigma_a + \sigma_s \exp[(\sigma_a + \sigma_s)D]}, \quad (5)$$

where σ_a is the direct impact amorphization cross section and σ_s is the defect stimulated amorphization cross section. The Hecking model also gives excellent fits for the simulated functions, as can be seen in Fig. 13. For all different recoil energy distributions the direct impact cross section is much smaller than the defect stimulated cross section (Table VI). Moreover, the fact that the cross section ratio σ_s/σ_a is higher for the 3 eV–2 keV case (about 8) than for the 15 eV–2 keV case (about 6) supports the idea that low-energy recoils recombine defects mostly outside amorphous regions (since the growth of amorphous regions is suppressed less by 3–15 eV recoils than direct impact amorphization).

TABLE VI. The fitted parameters for ion-irradiation-induced amorphization of Si for Wang and Hecking amorphization models. Simulated (consisting of 3 eV–2 keV or 15 eV–2 keV recoils) and monoenergetic (100-eV or 1-keV) recoil distributions were used. The Tersoff-III potential model was used. In the Wang model (direct impact with crystallization) the A parameter is the crystallization efficiency and k parameter is the amorphization cross section. For the Hecking model (direct impact/defect stimulated), σ_a is the direct impact amorphization cross section and σ_s is the defect stimulated amorphization cross section.

Model	Recoils		
		A	$k = D_n/D$
Wang	3 eV–2 keV	0.9002 ± 0.0002	3.822 ± 0.009
	15 eV–2 keV	0.8667 ± 0.0008	6.326 ± 0.049
	100 eV	0.8916 ± 0.0004	5.860 ± 0.024
	1 keV	0.7746 ± 0.0010	2.231 ± 0.013
		σ_a	σ_s
Hecking	3 eV–2 keV	0.0553 ± 0.0003	0.447 ± 0.002
	15 eV–2 keV	0.1567 ± 0.0026	0.928 ± 0.013
	100 eV	0.0990 ± 0.0009	0.731 ± 0.005
	1 keV	0.1448 ± 0.0016	0.480 ± 0.006

We find that both the models of Wang *et al.*[18] and Hecking and co-workers[4,15] produce good fits to the development of the amorphous fraction during ion irradiation. The Hecking model describes the amorphization process better, since the Wang model takes only the direct impact amorphization into account (the simulations have shown that also isolated defects are produced in individual cascades in silicon.[7,34]) However, some information about the crystallization during the amorphization process can be extracted using this model. The expansion of the Hecking model by Weber[15] would describe the process even better, but some other measure of the nature of the amorphous state, in addition to the structure factor used now, would be needed to enable a fit to this model. We have not found another independent measure that could be used for this fitting.

We thus conclude that the amorphization of Si proceeds mainly via growth of amorphous pockets. The direct impact amorphization is suppressed by the low-energy recoil recrystallization, since isolated defect clusters are easier to anneal than large amorphous regions.

B. Structure of amorphous Si and Ge

Because the volume changes for different potentials of the same material showed large variation, we cannot predict the

density of amorphous materials conclusively. Moreover, the final volume of the irradiated cells was found to depend on the recoil energy distribution. Monoenergetic 100-eV recoil distribution produced a very similar structure as the variable energy distribution, whereas monoenergetic 1-keV distribution produced a slightly denser material. Nevertheless, the coordination numbers and bond lengths were very close for each distribution and different from the molten ones. The amorphization doses were in a reasonable agreement with the experiments.

The initial direction distribution of recoil atoms had no effect on the final structure of the irradiated cells. Also the relaxation method, either three dimensional (3D) or in the z direction only, did not affect the final structure. However, a bigger dose is needed until the volume of the z-relaxed cells reaches a steady state, because it takes longer for the amorphous material to flow and relax the pressure induced in the cell by the phase transition.

Ab initio simulations of the structure of a-Si frequently find a much larger fraction of defects ($\sim 10\%$) than what is observed experimentally ($\lesssim 1\%$).[64–66] The defects in these simulations take the form of, e.g., threefold and fivefold coordinated atoms, as well as three-membered, four-membered, etc. atom rings.[65,66] The a-Si structure in *ab initio* simulations was usually created by extremely rapid quenching, typically over ~ 1 ps, due to the limited time scale available to quantum-mechanical simulations. Since the cooling in collision cascades in semiconductors also occurs over 1–2 ps, it is not surprising that the defects observed in the *ab initio* modeling are similar to those we observe in irradiated Si. The fact that we observe similar defects as the *ab initio* calculations gives us confidence that the defects we observe can be expected to exist at least at low temperatures. Since we observe much less defects in the quenched a-Si cells, it also seems clear that the predominant reason for the presence of high defect concentrations in irradiated Si is the very rapid cooling of the amorphous zones produced.

Custer *et al.* report that the density of the amorphous structures they produced by irradiation did not change during annealing,[19] and that it is about 2% lower than the density of the crystalline phase. In our annealing tests, the EDIP potential and Tersoff potentials both had a fairly stable volume (about 2–3 % higher than that of the crystalline phase) during annealing between 600 K and the melting point, and a similar volume in the quenched cells. The density for no annealing and low-temperature anneals was different, but this is probably because very unstable defects can be present in cells simulated only for short time scales at low temperatures, and these would anneal out on any experimental time scale. Thus we can consider the results of the T-III and EDIP potential to be in a good agreement with experiments. The fact that both the quenched and ion-beam-amorphized and annealed a-Si that we observe with these potentials still contain coordination defects strongly supports the suggestion by Custer *et al.*[19] that a-Si cannot only contain tetrahedrally coordinated atoms.

High-energy defects, not appearing in quenched amorphous material, were present in irradiated cells for all the potential models and materials tested. In irradiated a-Si many more three- and four-membered rings were present than in molten a-Si. These rings were associated with peaks near 60° and 75° in the bond-angle distributions.

Our simulations predict an increase in coordination number and bond length during ion-beam amorphization of Si. Although some previous experiments have reported coordination numbers above 4, the most recent results indicate that this is an artifact due to a too small cutoff in reciprocal space,[67,68] and report a first-shell coordination number of 3.88 (Ref. 68). No bond-length increase was observed in these experiments. Although the discrepancy between our simulations and experiments might again be a result of our short simulation times, it does not seem likely that the average coordination number would go from a value above 4 to a value below 4 even for very long time scales. Hence, it appears that the empirical potentials we use do not reproduce the experimental coordination numbers in ion-beam-amorphized Si correctly. The reason for this is most likely related to the reported presence of about 1% vacancylike defects associated with dangling bonds in ion-beam-amorphized Si.[28] Such defects will lower the average coordination number. For some reason these defects do not appear to be formed in large numbers in our simulations, leading to a higher coordination number.

For irradiated Ge an ion dose dependent increase in bond length is experimentally observed,[50] in agreement with our results, but the experimental increase is smaller.

C. Structure of $a-$GaAs

The volume of our a-GaAs (4.5% less dense than c-GaAs) agrees well with the experimental value of about 4% (Ref. 69).

It is not experimentally clear whether wrong bonds (i.e., bonds between like atoms) are present in a-GaAs. The fraction of wrong bonds has been experimentally measured to be between 0% and 12%.[69–76] It has been suggested that wrong bonds could not be present in a-GaAs because of the energy cost associated with them.[77] However, irradiated amorphous structures do contain high-energy defects, which might contain wrong bonds.

The comparison of the bonding structure with experiments is complicated by the presence of the 2.8-Å-long "metallic"[53] Ga-Ga bonds in our simulations. If such bonds existed in *as large* amounts as we see in our simulations, they should have been observed in the experiments of Ridgway *et al.*[69] But if they are present in much smaller numbers, the experimental sensitivity may not be good enough to detect them. During 400-ps annealing at 900 K, the number of Ga-Ga bonds was reduced by 16%, and especially the bonds longer than 2.7 Å seem to decrease in number (Fig. 11). Therefore, the majority of these bonds are probably eliminated on experimentally accessible time scales, leaving open the possibility that some are present in real GaAs as well.

If only bonds shorter than 2.7 Å are counted, the fraction of wrong bonds we observe before annealing is 14%, which is close to the range of values 0–12 % observed in the experiments.[69–76]

The coordination number (again with 2.7 Å cutoff) of 3.45 we obtained for irradiated a-GaAs is smaller than the experimental value of 3.85 measured by extended x-ray-absorption fine structure (EXAFS).[69,12] An increase in the nearest-neighbor distance was observed in the EXAFS measurements, from 2.445 Å in the crystal to 2.452 Å in the amorphous phase. We observe the same effect in our simulations (2.45 Å in the crystal vs 2.51 Å in the amorphous zone), but the experimental increase was much smaller.

Since both deviations (fraction of wrong bonds and coordination number) from the values of perfect c-GaAs are smaller in experiments, our simulated a-GaAs cell has more defects than the samples measured by Ridgway *et al.*[69] This difference may, again, be related to annealing effects. In the experiments the sample was not kept at low temperatures before analysis. It is known that structural changes can occur in GaAs even at room temperature,[78,79] so it is likely that some of the defects in our simulated cells would vanish during experimentally accessible time scales. During our high-temperature annealing tests the Ga-As bonds were shortened from 2.51 Å to 2.48 Å.

To summarize our discussion of the structure of a-GaAs, we have found that our simulations reproduce at least qualitatively correctly several experimentally observed features (density change, coordination number less than 4, average bond length, presence of wrong bonds in some samples). The fact that we observe weak ''metallic'' Ga-Ga bonds around 2.8–2.9 Å leads us to propose that such bonds exist in irradiated a-GaAs at least at low temperatures.

V. CONCLUSIONS

We have studied ion-irradiation-induced amorphization of Si, Ge, and GaAs by simulating the entire amorphization process starting from a perfect crystal until a stable amorphous state is reached. Comparison of results obtained with different interatomic potential models in the same material and comparison with experiment allowed us to deduce which features observed in the simulations can be considered reliable.

We showed that very low-energy recoils ($\sim$3–15 eV) can lead to a significant athermal dynamic recrystallization component during ion irradiation.

From the development of volume and potential energy during ion irradiation we deduced that the volume of the material is not a good measure of whether the material is fully amorphized.

The amorphization doses, bond lengths, and average coordination numbers were in most cases found to behave at least qualitatively similarly as in experiments. The main exception is the coordination number of a-Si, for which the experimentally observed value of less than 4 (Ref. 68) is not reproduced by any of the models used.

In the amorphous zones produced during irradiation, coordination defects were very common. We also observed a large fraction of topological defects, such as three-membered, four- membered, etc. atom rings in the amorphous network. In particular, in irradiated a-Si, triangles with all angles close to 60° are very common. During annealing most, but not all, of these defects were removed. We propose that these defects are those suggested to be present in ion-beam-amorphized Si by Custer *et al.*[19]

Our results also suggest that weak Ga-Ga bonds whose lengths are near 2.8 Å are present in irradiated a-GaAs.

ACKNOWLEDGMENTS

We thank Dr. M. Ridgway, Dr. C. Glover, and Professor M. Bazant for useful discussions, and Mr. J. Peltola for calculating the recoil spectra of high-energy ions. The research was supported by the Academy of Finland under Project No. 44215. Grants for computer time from the Center for Scientific Computing in Espoo, Finland are gratefully acknowledged.

[1] J. R. Dennis and E. B. Hale, J. Appl. Phys. **49**, 1119 (1978).
[2] J. Narayan, D. Fath, O. S. Oen, and O. W. Holland, J. Vac. Sci. Technol. A **2**, 1303 (1984).
[3] M. O. Ruault, J. Chaumont, J. M. Penisson, and A. Bourret, Philos. Mag. A **50**, 667 (1984).
[4] N. Hecking, K. F. Heidemann, and E. T. Kaat, Nucl. Instrum. Methods Phys. Res. B **15**, 760 (1986).
[5] T. Motooka and O. W. Holland, Appl. Phys. Lett. **58**, 2360 (1991).
[6] S. U. Campisano, S. Coffa, V. Rainieri, F. Priolo, and E. Rimini, Nucl. Instrum. Methods Phys. Res. B **80/81**, 514 (1993).
[7] M.-J. Caturla, T. Diaz de la Rubia, L. A. Margués, and G. H. Gilmer, Phys. Rev. B **54**, 16 683 (1996).
[8] L. J. Lewis and R. M. Nieminen, Phys. Rev. B **54**, 1459 (1996).
[9] K. Nordlund and R. S. Averback, Phys. Rev. B **56**, 2421 (1997).
[10] B. Weber, D. M. Stock, K. Gärtner, and C. Wende, Radiat. Eff. Defects Solids **141**, 161 (1997).
[11] A. Gaber, H. Zillgen, P. Ehrhart, P. Partyka, and R. S. Averback, J. Appl. Phys. **82**, 5348 (1997).
[12] M. C. Ridgway, C. J. Glover, E. Bezakova, A. P. B. G. J. Foran, and K. M. Yu, Nucl. Instrum. Methods Phys. Res. B **148**, 391 (1999).
[13] K. M. Beardmore and N. Gronbech-Jensen, Phys. Rev. B **60**, 12 610 (1999).
[14] M. Koster and H. M. Urbassek, Phys. Rev. B **62**, 11 219 (2000).
[15] W. J. Weber, Nucl. Instrum. Methods Phys. Res. B **166-167**, 98 (2000).
[16] L. Malerba and J. M. Perlado, J. Nucl. Mater. **289**, 57 (2001).
[17] F. Gao, W. J. Weber, and R. Devanathan, Nucl. Instrum. Methods Phys. Res. B **140**, 176 (2001).
[18] S. X. Wang, L. M. Wang, and R. C. Ewing, Phys. Rev. B **63**, 024105 (2001).
[19] J. S. Custer, M. O. Thompson, D. C. Jacobson, J. M. Poate, S. Roorda, W. C. Sinke, and F. Spaepen, Appl. Phys. Lett. **64**, 437 (1994).

[20] S. Kugler, L. Pusztai, L. Rosta, P. Chieux, and R. Bellisent, Phys. Rev. B **48**, 7685 (1993).
[21] B. R. Djordjevic, M. F. Thorpe, and F. Wooten, Phys. Rev. B **52**, 5685 (1995).
[22] M. J. Caturla, T. Diaz de la Rubia, and G. H. Gilmer, J. Appl. Phys. **77**, 3121 (1995).
[23] D. M. Stock, G. H. Gilmer, M. Jaraíz, and T. Diaz de la Rubia, Nucl. Instrum. Methods Phys. Res. B **102**, 207 (1995).
[24] B. Weber, D. M. Stock, and K. Gärtner, Nucl. Instrum. Methods Phys. Res. B **148**, 375 (1999).
[25] K. Gärtner and B. Weber, Nucl. Instrum. Methods Phys. Res. B **180**, 274 (2001).
[26] In the study by Beardmore and Gronbech-Jensen[13] the density of the amorphized material depends on the pressure coupling constant τ_p.
[27] H. J. C. Berendsen, J. P. M. Postma, W. F. van Gunsteren, A. DiNola, and J. R. Haak, J. Chem. Phys. **81**, 3684 (1984).
[28] S. Roorda, R. A. Hakvoort, V.-A. van, P. A. Stolk, and F. W. Saris, J. Appl. Phys. **72**, 5145 (1992).
[29] K. Nordlund, Comput. Mater. Sci. **3**, 448 (1995).
[30] A presentation of the MDRANGE computer code is available at the website http://beam.helsinki.fi/~knordlun/mdh/mdh_program.html
[31] M.-J. Caturla, T. Diaz de la Rubia, and G. H. Gilmer, in *Materials Synthesis and Processing Using Ion Beams*, edited by R. J. Culbertson *et al.*, MRS Symposia Proceedings No. **316** (Materials Research Society, Pittsburgh, 1994), p. 141.
[32] J. Tarus, K. Nordlund, A. Kuronen, and J. Keinonen, Phys. Rev. B **58**, 9907 (1998).
[33] T. Diaz de la Rubia and G. H. Gilmer, Phys. Rev. Lett. **74**, 2507 (1995).
[34] K. Nordlund, M. Ghaly, R. S. Averback, M. Caturla, T. Diaz de la Rubia, and J. Tarus, Phys. Rev. B **57**, 7556 (1998).
[35] H. Hensel and H. M. Urbassek, Phys. Rev. B **57**, 4756 (1997).
[36] K. Nordlund, J. Nord, and J. Keinonen, Nucl. Instrum. Methods Phys. Res. B **175-177**, 31 (2000).
[37] K. Nordlund, J. Peltola, J. Nord, J. Keinonen, and R. S. Averback, J. Appl. Phys. **90**, 1710 (2001).
[38] F. H. Stillinger and T. A. Weber, Phys. Rev. B **31**, 5262 (1985).
[39] J. Tersoff, Phys. Rev. B **38**, 9902 (1988).
[40] M. Z. Bazant and E. Kaxiras, Phys. Rev. Lett. **77**, 4370 (1996).
[41] M. Z. Bazant, E. Kaxiras, and J. F. Justo, Phys. Rev. B **56**, 8542 (1997).
[42] J. F. Justo, M. Z. Bazant, E. Kaxiras, V. V. Bulatov, and S. Yip, Phys. Rev. B **58**, 2539 (1998).
[43] K. Ding and H. C. Andersen, Phys. Rev. B **34**, 6987 (1986).
[44] J. Tersoff, Phys. Rev. B **39**, 5566 (1989); **41**, 3248 (1990).
[45] K. Albe, K. Nordlund, J. Nord, and A. Kuronen (unpublished).
[46] R. S. Averback and T. Diaz de la Rubia, in *Solid State Physics*, edited by H. Ehrenfest and F. Spaepen (Academic Press, New York, 1998), Vol. 51, pp. 281–402.
[47] The glass temperature was obtained by simulating a 2000-atom cell with disordered structure at temperatures between 100 and 1600 K with a 20-K interval. At 1200 K the derivative of the thermal-expansion coefficient changed dramatically (and even changed sign), which is a signature of the glass temperature.[80] However, because of the limited time scale of the equilibration runs at each temperature, this can only be considered to be an upper limit for the glass temperature.
[48] M. C. Ridgway and C. J. Glover, Phys. Rev. B **61**, 12 586 (2000).
[49] G. Kresse and J. Hafner, Phys. Rev. B **49**, 14 251 (1994).
[50] C. J. Glover, M. C. Ridgway, K. M. Yu, G. J. Foran, D. Desnica-Frankovic, C. Clerc, J. L. Hansen, and A. Nylandsted-Larsen, Phys. Rev. B **63**, 073204 (2001).
[51] J. F. Ziegler, SRIM96 computer code (private communication, 1996).
[52] W. Wesch, E. Wendler, G. Götz, and N. P. Kekelidse, J. Appl. Phys. **65**, 519 (1989).
[53] X. G. Gong, G. L- Chiarotti, M. Parrinello, and E. Tosatti, Phys. Rev. B **43**, 14 277 (1991).
[54] H. Zillgen and P. Ehrhart, Nucl. Instrum. Methods Phys. Res. B **127-128**, 27 (1996).
[55] P. Ehrhart and H. Zillgen, in *Defects and Diffusion in Silicon Processing*, edited by T. Diaz de la Rubia, S. Coffa, P. A. Stolk, and C. S. Rafferty, MRS Symposia Proceedings No. **469** (Materials Research Society, Pittsburgh, 1997), p. 175.
[56] P. Partyka, Y. Zhong, K. Nordlund, R. S. Averback, I. K. Robinson, and P. Ehrhart, Phys. Rev. B **64**, 236207 (2001).
[57] A. Polity and F. Rudolf, Phys. Rev. B **59**, 10 025 (1999).
[58] K. Saarinen, S. Kuisma, J. Mäkinen, P. Hautojärvi, M. Törnqvist, and C. Corbel, Phys. Rev. B **51**, 14 152 (1995).
[59] S. Kuisma, K. Saarinen, P. Hautojärvi, and C. Corbel, Phys. Rev. B **55**, 9609 (1997).
[60] M. D. Kluge, J. R. Ray, and A. Rahman, Phys. Rev. B **36**, 4234 (1987).
[61] M. Tang, L. Colombo, J. Zhu, and T. Diaz de la Rubia, Phys. Rev. B **55**, 14 279 (1997).
[62] E. Glaser, T. Fehlhaber, and B. Breeger, Nucl. Instrum. Methods Phys. Res. B **148**, 426 (1999).
[63] R. D. Goldberg, J. S. Williams, and R. G. Elliman, Phys. Rev. Lett. **82**, 771 (1999).
[64] R. Car and M. Parrinello, Phys. Rev. Lett. **60**, 204 (1988).
[65] D. A. Drabold, P. A. Fedders, O. F. Sankey, and J. D. Dow, Phys. Rev. B **42**, 5135 (1990).
[66] P. A. Fedders, D. A. Drabold, and S. Klemm, Phys. Rev. B **45**, 4048 (1992).
[67] K. Laaziri, S. Kycia, S. Roorda, M. Chicoine, J. L. Robertson, J. Wang, and S. C. Moss, Phys. Rev. Lett. **82**, 3460 (1999).
[68] K. Laaziri, S. Kycia, S. Roorda, M. Chicoine, J. L. Robertson, J. Wang, and S. C. Moss, Phys. Rev. B **60**, 13 520 (1999).
[69] M. C. Ridgway, C. J. Glover, G. J. Foran, and K. M. Yu, J. Appl. Phys. **83**, 4610 (1998).
[70] D. Udron, M. L. Theye, D. Raoux, A. M. Flank, P. Lagarde, and J. P. Gaspard, J. Non-Cryst. Solids **137&138**, 131 (1991).
[71] D. Udron, A. Fland, P. Lagarde, D. Raoux, and M. L. Theye, J. Non-Cryst. Solids **150**, 361 (1992).
[72] S. H. Baker, M. I. Mansor, S. J. Gurman, S. C. Bayliss, and E. A. Davis, J. Non-Cryst. Solids **144**, 63 (1992).
[73] C. Senemaud, E. Belin, A. Gheorghiu, and M. Theye, Solid State Commun. **55**, 947 (1985).
[74] R. J. Temkin, Solid State Commun. **15**, 1325 (1974).
[75] N. J. Shevchik, J. Tejeda, and M. Cardona, Phys. Rev. B **9**, 2627 (1974).
[76] N. J. Chevchik and W. Paul, J. Non-Cryst. Solids **13**, 1 (1973).
[77] N. Mousseau and L. J. Lewis, Phys. Rev. Lett. **78**, 1484 (1997).

[78] M. W. Bench, I. M. Robertson, and M. A. Kirk, in *Proceedings of the 46th Annual Meeting of the Electron Microscopy Society of America*, edited by G. W. Bailey (San Fransisco Press, San Fransisco, CA, 1988), p. 760.
[79] M. W. Bench, I. M. Robertson, M. A. Kirk, and I. Jenčič, J. Appl. Phys. **87**, 49 (2000).
[80] J. W. D. Callister, in *Materials Science and Engineering: An Introduction*, 5th ed. (Wiley, New York, 1999), Chap. 14.